Chinese Chemical Letters 34 (2023) 107689

Contents lists available at ScienceDirect

Chinese Chemical Letters

journal homepage: www.elsevier.com/locate/cclet

Hydrogen-bond locked purine chromophores with high photostability for lipid droplets imaging in cells and tissues

Jinlin Zhou[a], Kun Li[a], Lei Shi[b], Hong Zhang[a], Haoyuan Wang[a], Yimin Shan[a], Shanyong Chen[a,*], Xiao-Qi Yu[a,c,*]

[a] Key Laboratory of Green Chemistry and Technology, Ministry of Education, College of Chemistry, Sichuan University, Chengdu 610064, China
[b] State Key Laboratory of Oral Diseases, West China Hospital of Stomatology, Sichuan University, Chengdu 610064, China
[c] Department of Chemistry, Xihua University, Chengdu 610039, China

ARTICLE INFO

Article history:
Received 8 May 2022
Revised 11 July 2022
Accepted 15 July 2022
Available online 28 July 2022

Keywords:
Fluorescent probe
Purine
Hydrogen bond
Lipid droplets
Fatty liver

ABSTRACT

Recently, hydrogen-bonding has attracted extensive attention in the design of chromophores. Here, a new class of hydrogen-bond locked purine chromophores (HOPs) were reported by introducing a hydroxyphenyl group into the C(6) position of purine. The intramolecular hydrogen bond plays a dominant role to light up these probes. As a bonus, HOPs show high photostability. Moreover, HOPs exhibit remarkable capability for the specific lipid droplets imaging in living cells with excellent biocompatibility and are also potential for diagnosing fatty liver diseases. These results bring important new insights into the photophysics of the purine-based chromophores and provide a new scaffold with high photostability for bioimaging.

Hydrogen bond (HB) is extensively adopted by nature to implement some biological dynamic processes, such as proton transfer (PT) concomitant charge transfer (CT) in proteins and enzymes of photosynthesis and respiration, which play crucial roles in organisms [1–4]. HB dynamics, especially those occurring on electronic excited states, could tune and regulate photophysical and photochemical properties of many photofunctional molecules [5–9]. Therefore, HB is widely applied in the design of chromophores for biosensing and bioimaging. Green fluorescent protein (GFP) is extensively used in life sciences and molecular biology as a genetically encoded fluorescent tag [10]. However, natural protein-free GFP analogues suffer from emission quenching by protic solvent [11]. In recent years, some artificial GFP derivatives have been reported by forming intramolecular hydrogen-bond based on the excited-state intramolecular proton transfer (ESIPT) process to enhance fluorescence emissions and realize remarkable red shifts [12]. Furthermore, strengthening of intermolecular HB could provide an extra stabilization to realize lower excitation energy, which even makes the single benzene fluorophores display a remarkable red emission [13]. Intermolecular HB formed between chromophores and solvent molecules also affect fluorescence emissions, providing opportunities for bioimaging. For example, the Xu group reported an intermolecular HB sensitive fluorogenic probe for super-resolution imaging of lipid droplets (LDs). The Naphthalimide-based chromophore can form intermolecular HBs with protic media in cytochylema, resulting in low fluorescence emission, while in LDs, it elicits bright fluorescence [14,15].

Similar to GFP chromophore, purine is a vital biological molecule unit of DNA and RNA, which has been used as anticancer, antiviral drugs, and receptor antagonists due to its biological importance [16–18]. Besides its good biocompatibility, the purine core structure has a large π-conjugated plane with multiple functional modification sites, which makes it attractive for designing fluorophores in biological imagining. In the previous works, we have reported a family of purine-based chromophores (Scheme 1, upper, left), which show good potential for the specific imaging of organelles, such as lipid droplets, plasma membranes, and endoplasmic reticulum [19–21]. However, the photostability and quantum yields (Φ_F) of these probes still need to be improved. Inspired by reported excellent probes involving hydrogen bonding, we set out to reconstruct purine-based chromophores using the hydrogen bonding strategy and expected that these probes exhibit improved fluorescence properties.

The structure of new purine-based chromophores was outlined in Scheme 1. The introduction of a hydroxyphenyl into purine was expected to form a six-membered ring through hydrogen bonding, which can regulate the photophysical properties of these

* Corresponding authors at: Key Laboratory of Green Chemistry and Technology, Ministry of Education, College of Chemistry, Sichuan University, Chengdu 610064, China.
E-mail addresses: chensy@scu.edu.cn (S. Chen), xqyu@scu.edu.cn (X.-Q. Yu).

https://doi.org/10.1016/j.cclet.2022.07.032
1001-8417/

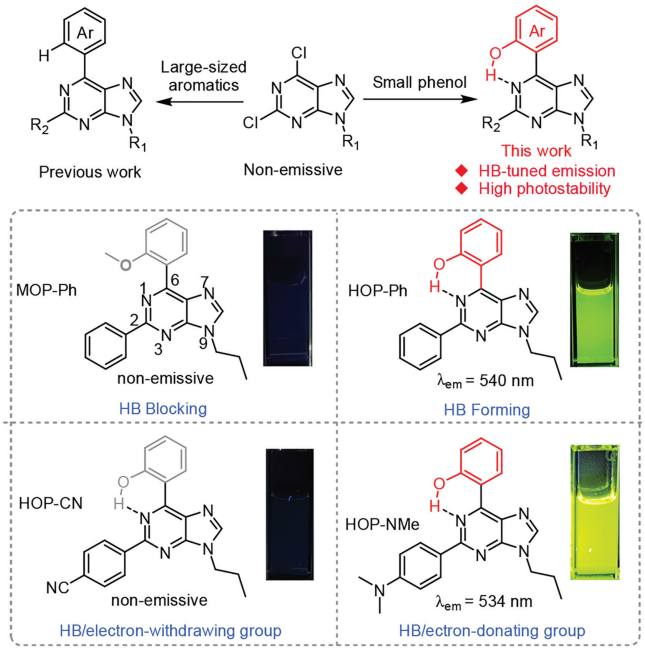

Scheme 1. Structure of the purine chromophores along with photographic images of toluene solution samples taken under a 365 nm UV lamp.

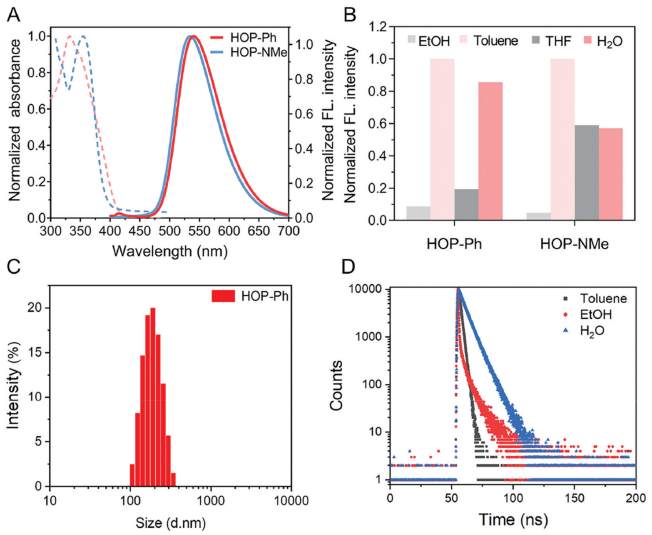

Fig. 2. (A) Normalized fluorescence spectra of HOP-Ph and HOP-NMe (5 μmol/L) in aqueous media; (B) Normalized fluorescence intensities of HOP-Ph and HOP-NMe in different solvents; (C) Average hydrodynamic size of HOP-Ph (10 μmol/L, in PBS containing 1% DMSO) determined by DLS measurement; (D) Fluorescence decay curves of HOP-Ph in EtOH, toluene, and H_2O.

chromophores [22]. Indeed, we found that these hydrogen-bond locked purine chromophores have high Φ_F in nonpolar media or aggregation state [23,24] and show high photostability [25]. Moreover, HOPs exhibit remarkable capability for the specific lipid droplets imaging in living cells with excellent biocompatibility and are also potential for diagnosing fatty liver diseases.

A propyl group was first introduced into the purine skeleton through N^9-alkylation, and then followed by Suzuki-Miyaura cross-coupling reaction [26] afforded all the purine derivatives (Scheme S1 in Supporting information). MOP-Ph in which the hydroxyl group is replaced with methoxy group was prepared to serve as the reference compound of HOP-Ph. HOP-NMe and HOP-CN were further prepared to investigate the electronic effects on fluorescence emissions. All the compounds were characterized by ^{1}H NMR, ^{13}C NMR, and high-resolution mass spectrometry (HRMS). The three HOPs probes were further confirmed by single crystal X-ray diffraction analysis (Fig. 1 and Fig. S1 in Supporting information). As shown in Fig. 1, the torsion angles of the phenol ring with purine core are in a small range varied from 2.81° to 8.69°, implying that the purine-based probes have approximate planar conformations. The distances of the hydroxyl proton and N(1) increased with the electron-withdrawing ability. Namely, the hydrogen bond with 1.823 Å of N-H distance in HOP-CN is the weakest among them. The nearly planar conformations together with N-H distances support the existence of a six-membered ring intramolecular hydrogen bond. The proton of hydroxyl bonds

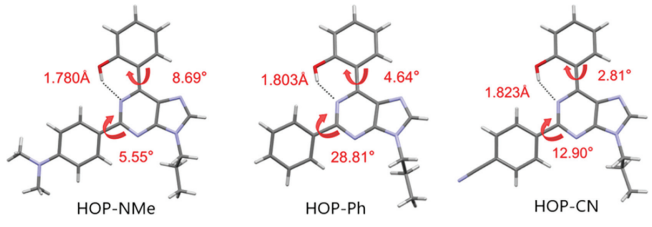

Fig. 1. Single-crystal structures of HOP-NMe, HOP-Ph and HOP-CN. Carbon, hydrogen, nitrogen, and oxygen atoms are shown in gray, blue, mauve, red, respectively.

selectively with N(1) rather than N(7) of the purine, which may be ascribed to the lower energy of a six-membered ring compared to a seven-membered ring.

The photophysical properties of HOP probes and the reference compound MOP-Ph were investigated. As shown in Fig. S2 (Supporting information), the four compounds display obvious absorption bands varied between 300 and 400 nm. Fluorescence emission spectra were measured in several solvents (Fig. 2A and Fig. S3 in Supporting information). As expected, the reference compound MOP-Ph is non-emissive, demonstrating the necessity of intramolecular hydrogen bond to light up HOPs. HOP-CN bearing an electron-withdraw CN group on the benzene ring is also non-emissive. In stark contrast to MOP-Ph and HOP-CN, HOP-Ph and HOP-NMe are emissive and show similar fluorescence properties. Specifically, HOP-Ph and HOP-NMe elicit strong emissions peaked around 530 nm in nonpolar solvent like toluene and have weak emissions in polar solvents including EtOH and THF. Giving the neutral and non-polar lipid environment inside LDs, HOP-Ph and HOP-NMe should be good candidates for LDs imaging. The fluorescence intensity of HOP-Ph and HOP-NMe increase dramatically with the increase of H_2O or toluene with no obvious change of emission-shift, when the ratio of H_2O or toluene exceed 90% (Fig. S4 in Supporting information). Although H_2O is a polar solvent, the two compounds have similar fluorescence intensity with that in toluene (Fig. 2B). Dynamic light scattering (DLS) data shows that the two compounds exist with aggregate states (118–178 nm) in water (Fig. 2C and Fig. S5 in Supporting information). Due to the restriction of intramolecular motions (RIM) mechanism in the aggregated state, the molecular conformation would be coplanar, which is beneficial for forming intramolecular HB and promoting radiative pathway [27,28].

Quantum yields and lifetime were further tested. The fluorescence quantum yields (Φ_F) in solutions (THF, EtOH, toluene) and in aggregations (H_2O) are summarized in Table S1 (Supporting information). The quantum yields of HOP-Ph, HOP-NMe in aqueous media and in toluene were relatively higher compared with those in polar solvents, like THF and EtOH. In nonpolar solvent like toluene, intramolecular HB is readily formed, which is beneficial to suppress non-radiative relaxation by locking the purine structure. In aprotic polar solvents like EtOH, intramolecular HB was weakened

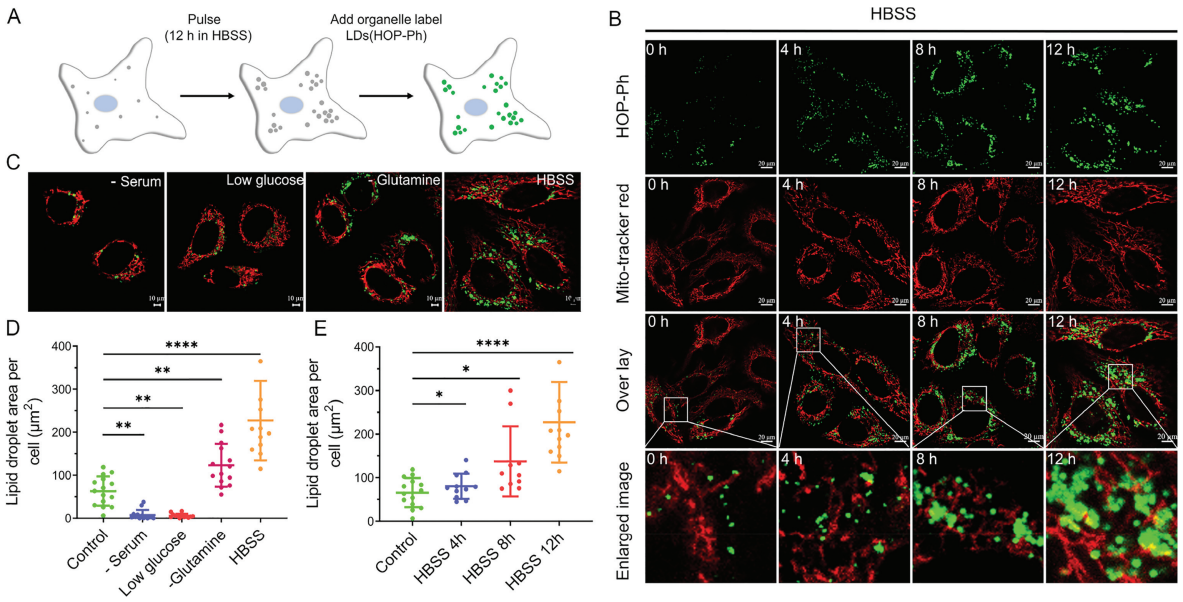

Fig. 3. (A) Illustration of the paradigm to visualize the stability of starvation-induced, clustered LDs. (B) HepG2 cells were grown in CM or HBSS for the indicated times, fixed, and analyzed by fluorescence microscopy. LDs were stained with HOP-Ph (5 μmol/L, green) for 25 min, mitochondria with Mitochondria Tracker Red (1 μmol/L, red) for 15 min. (C) Cells deprived of the indicated groups of nutrients for 12 h were fixed, the distribution of LDs (green) and mitochondria (red) analyzed by fluorescence microscopy. (D) The LDs area per cell quantified in (C). (E) The abundance of LDs was quantified during incubations in CM (Control) or HBSS in (B). Images were acquired using 405 nm (green), and 543 nm (red), and emission windows of 500–600 nm (green), and 590–650 nm (red). Data in D and E are expressed as means ± SEM. $^{*}P < 0.05$; $^{**}P < 0.01$; $^{***}P < 0.001$; $^{****}P < 0.0001$.

by solvent molecules, therefore, weak emissions with low quantum yields were observed [29,30]. HOP-Ph and HOP-NMe exhibited weak emissions in THF, which might be ascribed to solute-solvent electron transition [31–33].

Fluorescence lifetime (τ) values of all the fluorophores are listed in Table S2 (Supporting information). HOP-Ph and HOP-NMe exhibited similar changes in average fluorescence lifetime towards different solvents. Taking HOP-Ph as an example, HOP-Ph has a shorter lifetime (0.23 ns) in EtOH than in other solvents (1.90 ns in TL; 6.34 ns in H_2O), and the lifetime decreased linearly with the increase of EtOH in toluene (Fig. 2D and Fig. S6 in Supporting information).

To further understand optical behavior, density functional theory (DFT) calculations were carried out, and their molecular frontier orbitals and detailed calculation results were summarized in Figs. S7, S8 and Tables S3 and S4 (Supporting information). The excited state calculation results revealed that electron densities of HOMO for HOP-Ph are distributed on the phenolic hydroxyl group and the central purine core, while in the LUMO, they are distributed on the benzene ring as well as the purine core. Electrostatic potential comparison between HOP-NMe, HOP-Ph, and HOP-CN indicates that electron donor group can remarkably increase the electron intensity of N(1) of purine core structures, meaning stronger hydrogen bonding, which explains the significant enhancement in the fluorescence quantum yield of HOP-NMe.

Considering the hydrophobic characteristic of HOP probes and lipophilic environment within LDs, we anticipated that the HB sensitive HOP probes could be used for LDs-targeted imaging in aprotic environment. Cytotoxicity of HOP probes on HepG2 cells was evaluated *via* CCK-8 assay before cell imaging, as shown in Fig. S9 (Supporting information). To evaluate the specificity of these HB locked purine-based probes towards LDs in live HepG2 cells, a commercially available LD-imaging agent Nile Red was used to costain with HepG2 cells (Fig. S10 in Supporting information). Photostability was an important factor for real-time imaging in living cells, so we further measured the photostability of HOPs. As shown in Fig. S11 (Supporting information), even after scanned 40 times, no significant decreasing of fluorescence intensity was observed in HOP-Ph. While the two commercial trackers were bleached completely, almost no fluorescence signal could be observed. Considering the Pearson correlation coefficient and photostability, HOP-Ph was selected to monitor the numbers and morphological changes of LDs under specific physiological conditions.

Throughout evolution, organisms have developed mechanisms to monitor and respond to fluctuations in nutrient abundance [34,35]. To get a better understanding of the dynamic changes in cellular LDs during starvation, we further used HOP-Ph to monitor the distribution and abundance of LDs in HepG2 cells under starvation. HepG2 cells were firstly incubated in complete serum containing rich medium (CM) and then transferred from CM into hank's balanced salt solution (HBSS). Finally, these cells were stained with HOP-Ph and mitochondria-tracker-red (MTR) (Fig. 3A). In contrast to CM, HBSS induced a rapid increasing in LDs levels that reached a higher steady-state level after 12 h. Ultimately, HBSS resulted in a 2.4-fold increase in the number of LDs compared to CM (Figs. 3B and E). We also observed the increase of LDs numbers and appearance with clusters in several human cell lines under HBSS starvation, such as HeLa and HL-7702 (Fig. S12 in Supporting information), suggesting that this phenomenon is a general cellular response to nutrient deprivation. HBSS starvation conditions have low concentrations of glucose and lack amino acids and serum. To understand the conclusive factors of LDs biogenesis, we selectively decrease some special groups of nutrients that are lacking in HBSS conditions. When HepG2 cells were incubated in media lacking serum or with low glucose, there is a severe decrease in LDs compared with CM (Figs. 3C and D). In contrast, incubation with media lacking glutamine, HepG2 cells increase the number of LDs, and this has a similar effect with HBSS starvation. These results have been explained that the generation of LDs during amino acid starvation is sufficient to induce autophagy-dependent LDs biogenesis *via* FAs recycling and avoiding the excess free FAs in cytoplasm to generate damaging bioactive lipids which is harmful to cells [36,37].

As the impressive cell imaging results in live cells and taking the advantage of the specificity of HOPs dyes, we investigated their ability to reveal lipid-rich organelles in mouse fatty tissues

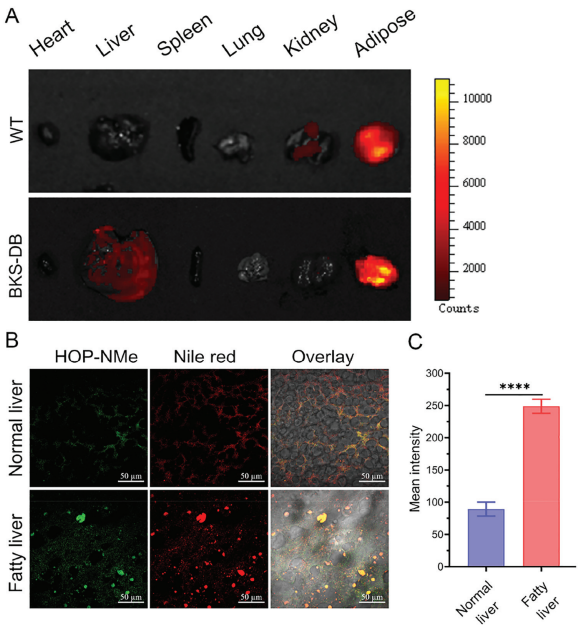

Fig. 4. Fluorescence images of mice and dissected organs, and the BKS-DB mice were intraperitoneally injected with HOP-NMe (5 μmol/L, 240 μL) for 1.5 h. (A) Fluorescence images of dissected organs. (B) Fluorescence images of WT and BKS-DB mouse liver slice co-stained with HOP-NMe and Nile Red. (C) Quantification of the relative mean fluorescence levels of normal and fatty liver tissues from the images of (B) with the green channel (HOP-NMe). Images were acquired using 405 nm (green), and 543 nm (red), and emission windows of 500–600 nm (green), and 610–700 nm (red).

imaging. We then chose the leptin receptor-deficient obese C57BLKS/J-db/db (BKS-DB) mouse to identify the fatty liver. Then the BKS-DB mouse was intraperitoneally injected with HOPs for 1.5 h, obvious fluorescence signals were detected on abdomen (Fig. S13 in Supporting information), and the organs including white adipose tissue were taken out for imaging and comparison with the wield type mouse (WT) (Fig. 4A and Fig. S14 in Supporting information). The adipose tissues and the liver had an observable strong fluorescence comparison with other organs. The adipose tissues were then imaged by fluorescence microscopy (Fig. S15 in Supporting information). The obtained results clearly revealed that HOP-NMe selectively stained the fat reservoirs of adipocytes and showed a remarkable ability of adipose tissues imaging. When we stained sliced WT and BKD-DB mouse liver tissues, using HOP-NMe and Nile red, in fatty liver tissues there is many LDs can be observed and quantitative analysis revealed a 1.8-fold increase in fluorescence intensity of BKS-DB to WT liver tissues in green channel (Figs. 4B and C). Hematoxylin and eosin stain also clearly showed abnormal lipid accumulation in the fatty liver tissues (Fig. S16 in Supporting information). These results showed that our probes specifically targeted LDs may be useful for monitoring the progression of metabolic syndrome induced by the increased lipid content.

In conclusion, a new series of intramolecular HB locked purine-based chromophores with switchable emissions (HB light up) and high photostability were devised. Furthermore, HOP probes could be applied for bioimaging with LDs in cells and fat liver tissues. As a new platform, HOP probes are potential for developing various selective markers or biosensors for subcellular organelle. Such a design strategy utilizing intramolecular HB can potentially be generalized for the preparation of purine chromophores with remarkable photophysical properties for subcellular organelle and tissue imaging.

Declaration of competing interest

The authors declare that they have no known competing financial interests or personal relationships that could have appeared to influence the work reported in this paper.

Acknowledgments

This work was financially supported by the National Natural Science Foundation of China (Nos. 22077088, 21877082, U21A20308) and the Foundation from the Science and Technology Department of Sichuan Province (Nos. 2020JDJQ0017, 2021YFH0132, 2020ZHCG0097). We also thank Yan-Hong Liu and Jing Li from the Comprehensive Training Platform of Specialized Laboratory in the College of Chemistry at Sichuan University for sample analysis.

Supplementary materials

Supplementary material associated with this article can be found, in the online version, at doi:10.1016/j.cclet.2022.07.032.

References

[1] C.L. Chen, Y.T. Chen, A.P. Demchenko, P.T. Chou, Nat. Rev. Chem. 2 (2018) 131–143.
[2] E. Odella, S.J. Mora, B.L. Wadsworth, et al., J. Am. Chem. Soc. 140 (2018) 15450–15460.
[3] J.N. Schrauben, M. Cattaneo, T.C. Day, A.L. Tenderholt, J.M. Mayer, J. Am. Chem. Soc. 134 (2012) 16635–16645.
[4] G.J. Zhao, K.L. Han, Acc. Chem. Res. 45 (2012) 404–413.
[5] T.S. Chu, J. Xu, J. Mol. Model. 22 (2016) 200.
[6] G. Kumar, K. Paul, V. Luxami, New J. Chem. 44 (2020) 12866–12874.
[7] A.C. Sedgwick, L. Wu, H.H. Han, et al., Chem. Soc. Rev. 47 (2018) 8842–8880.
[8] M. Chang, C. Yan, L. Shi, D. Li, W. Fu, Z. Guo, Chin. Chem. Lett. 33 (2022) 762–766.
[9] H. Liu, X. Cheng, Z. Bian, K. Ye, H. Zhang, Chin. Chem. Lett. 29 (2018) 1537–1540.
[10] M. Paolino, M. Gueye, E. Pieri, et al., J. Am. Chem. Soc. 138 (2016) 9807–9825.
[11] Y.H. Hsu, Y.A. Chen, H.W. Tseng, et al., J. Am. Chem. Soc. 136 (2014) 11805–11812.
[12] S. Chatterjee, K. Ahire, P. Karuso, J. Am. Chem. Soc. 142 (2020) 738–749.
[13] H. Kim, W. Park, Y. Kim, et al., Nat. Commun. 12 (2021) 5409.
[14] J. Chen, C. Wang, W. Liu, et al., Angew. Chem. Int. Ed. 60 (2021) 25104–25113.
[15] J. Chen, W.J. Liu, X.N. Fang, Q.L. Qiao, Z.C. Xu, Chin. Chem. Lett. 33 (2022) 5042–5046.
[16] F. Di Virgilio, Cancer Res. 72 (2012) 5441–5447.
[17] C. Lambertucci, M. Buccioni, D. Dal Ben, et al., Medchemcomm 6 (2015) 963–970.
[18] H. Xu, W. Chen, W. Zhang, L. Ju, H. Lu, New J. Chem. 44 (2020) 15195–15201.
[19] X. Liu, K. Li, L. Shi, et al., Chem. Commun. 57 (2021) 2265–2268.
[20] L. Shi, K. Li, L.L. Li, et al., Chem. Sci. 9 (2018) 8969–8974.
[21] L. Shi, Y.H. Liu, K. Li, et al., Angew. Chem. Int. Ed. 59 (2019) 9962–9966.
[22] Y. Chen, W. Zhang, Z. Zhao, et al., Angew. Chem. Int. Ed. 57 (2018) 5011–5015.
[23] M. Liu, W. Zhai, H. Chen, H. Zhang, C. Li, Anal. Chem. 92 (2020) 10792–10799.
[24] X. Wang, P. Li, Q. Ding, et al., J. Am. Chem. Soc. 141 (2019) 2061–2068.
[25] L.J. Karas, C.H. Wu, H. Ottosson, J.I. Wu, Chem. Sci. 11 (2020) 10071–10077.
[26] E. Rajanarendar, G. Mohan, E. Kalyan Rao, M. Srinivas, Chin. Chem. Lett. 20 (2009) 1–4.
[27] J.S. Ni, M.M.S. Lee, P. Zhang, et al., Anal. Chem. 91 (2019) 2169–2176.
[28] Y. Tu, J. Liu, H. Zhang, et al., Angew. Chem. Int. Ed. 58 (2019) 14911–14914.
[29] I.G. Alty, D.W. Cheek, T. Chen, et al., J. Phys. Chem. A 120 (2016) 3518–3523.
[30] S. Singha, D. Kim, B. Roy, et al., Chem. Sci. 6 (2015) 4335–4342.
[31] Y. Nagasawa, A.P. Yartsev, K. Tominaga, A.E. Johnson, K. Yoshihara, J. Am. Chem. Soc. 115 (1993) 7922–7923.
[32] A.O. Doroshenko, M.D. Bilokin, V.G. Pivovarenko, J. Photochem. Photobiol. A 163 (2004) 95–102.
[33] H. Pal, Y. Nagasawa, K. Tominaga, K. Yoshihara, J. Phys. Chem. 100 (1996) 11964–11974.
[34] A.S. Rambold, S. Cohen, J. Lippincott-Schwartz, Dev. Cell 32 (2015) 678–692.
[35] K.N. Wang, X.J. Peng, Y. Li, et al., Dyes Pigments 180 (2020) 108502.
[36] J. Kong, Y. Ji, Y.G. Jeon, et al., Nat. Commun. 11 (2020) 578.
[37] X. Wu, F. Geng, X. Cheng, et al., iScience 23 (2020) 101569.